

D14.5

Report on seismic testing -
Acerra



Funded by
the European Union

D14.5 Report on seismic testing - Acerra

Dissemination Level: Public

Lead Partner: UNINA

Due date: 31.03.2025

Actual submission date: 31.03.2025

PUBLISHED IN THE FRAMEWORK OF

MULTICARE (Horizon Europe grant 101123467)

AUTHORS

Carmine Moliterno, UNINA

Simone D'Amore, SUR

Nicolò Leccardi, RTB

Ciro Del Vecchio, UNINA

Marco Di Ludovico, UNINA

Stefano Pampanin, SUR

REVISION AND HISTORY CHART

| VERSION | DATE | EDITORS | COMMENT |
|---------|------------|--|---|
| V1 | 19.03.2025 | Nicolò Leccardi (RTB) | Draft (Connection system) |
| V2 | 22.03.2025 | Carmine Moliterno (UNINA) | Draft (Experimental tests) |
| V3 | 26.03.2025 | Simone D'Amore (SUR) | Draft (design of the low-damage exoskeleton, numerical simulations), and review of versions V1 and V2 |
| V4 | 27.03.2025 | Carmine Moliterno (UNINA) | Review of version V3 |
| V5 | 28.03.2025 | Carmine Moliterno (UNINA), Simone D'Amore (SUR) Nicolò Leccardi (RTB) Ciro Del Vecchio (UNINA) Marco Di Ludovico (UNINA) Stefano Pampanin (SUR) | Final Version |

DISCLAIMER

The information in this document is subject to change without notice. Company or product names mentioned in this document may be trademarks or registered trademarks of their respective companies.

All rights reserved

The document is proprietary of the COMMUNITAS consortium members. No copying or distributing, in any form or by any means, is allowed without the prior written agreement of the owner of the property rights.

This document reflects only the authors' view. The European Community is not liable for any use that may be made of the information contained herein. Responsibility for the information and views expressed in the therein lies entirely with the author(s).

Table of contents

| | |
|--|----|
| LIST OF FIGURES:..... | 4 |
| LIST OF TABLES:..... | 6 |
| 1. INTRODUCTION | 7 |
| 2. LOW-DAMAGE EXOSKELETON TECHNOLOGY | 7 |
| 3. EXPERIMENTAL TESTS | 9 |
| 3.1 Facilities of UNINA Laboratories..... | 9 |
| 3.1 Pseudo-Dynamic Tests..... | 11 |
| 4. CASE-STUDY BUILDING FOR PSEUDO-DYNAMIC TESTS..... | 13 |
| 4.1 Test set-up for Pseudo-Dynamic Tests (As-Built configuration)..... | 15 |
| 5. NUMERICAL SIMULATIONS FOR THE AS-BUILT CONFIGURATION..... | 17 |
| 5.1 Modelling Approach for the As-Built configuration | 17 |
| Member | 18 |
| 5.2 Selection of the record for NLTHAs | 19 |
| Earthquake..... | 20 |
| 5.3 Substructuring approach and results from NLTHAs | 20 |
| 6. METHODS FOR SEISMIC DESIGN OF THE LOW-DAMAGE EXOSKELETON..... | 23 |
| 7. NUMERICAL SIMULATIONS FOR THE RETROFITTED CONFIGURATION..... | 25 |
| 7.1 Application of the DBR procedure for the design of the exoskeleton | 25 |
| Mechanical property | 26 |
| 7.2 Test set-up for Pseudo-Dynamic Tests (Retrofitted Configuration) | 27 |
| 7.3 Substructuring approach and results from NLTHAs | 29 |
| 8. RESILIENT CONNECTION SYSTEMS | 29 |
| 8.1 Direct Anchorage (dowelled connections) | 30 |
| 8.2 T-Profile Connection System..... | 31 |
| 8.3 Bow-Tie Connection System | 31 |
| 9. REFERENCES..... | 32 |
| GLOSSARY | 35 |

LIST OF FIGURES:

| | |
|---|---|
| Figure 1. The Acerra demonstrator from outside..... | 7 |
| Figure 2. a) Schematic representation of the integrated rehabilitation based on low-damage timber-based exoskeletons, and b) seismic performance matrix with identification of the basic and enhanced design objective (modified after SEAOC [1] and Pampanin [2])..... | 8 |
| Figure 3. a) Example of experimental test on a beam-column joint based on the Pres-Lam technology [4], and b) NMIT Arts & Media Building realized by implementing the Pres-Lam technology [9]. | 8 |
| Figure 4. a) Example of a low-damage column-to-foundation connection, and b) hysteretic behaviour of the low-damage system considered (Pres-Lam), modified after fib [1]..... | 9 |

| | |
|--|----|
| Figure 5. Overview of the DiST laboratory and available facilities. | 10 |
| Figure 6. Shaking tables available at DiST laboratory. | 11 |
| Figure 7. Overview of the CeSMA laboratory and available facilities. | 11 |
| Figure 8. Pseudo-dynamic testing procedure. | 12 |
| Figure 9. Bonefro building damaged during the San Giuliano di Puglia Earthquake (left), with identification of a brittle shear failure in the RC column due to interaction between the RC frame and the masonry infills, modified after [12]. | 13 |
| Figure 10. Geometric characteristics of the considered building in terms of plan and lateral view, together with the identification of the substructured frame. | 14 |
| Figure 11. Test set-up: Front view. | 15 |
| Figure 12. Test set-up: Lateral view. | 16 |
| Figure 13. RC frame geometry and reinforcement details. | 17 |
| Figure 14. Results of the calibration of the Pivot hysteresis model parameters for an external beam-column joint (left), and for an internal one (right). Modified after Pampanin et al. [18]. | 18 |
| Figure 15. Modelling approach for existing RC infilled frame buildings. Modified after Moliterno et al. [17] and D'Amore & Pampanin [20]. | 19 |
| Figure 16. a) Spectrum of the selected record (red) compared with the other spectra from the spectrum-compatibility procedure (gray) and the code-spectrum for the city of Bonefro at LSLS, and b) accelerogram of the selected record. | 20 |
| Figure 17. Modal participating mass from the modal analysis of the numerical model of the whole building. | 21 |
| Figure 18. a) Floor push-over curves obtained both for the whole building as well as for the substructured frame, and b) ratio between the stiffness of the whole building and that of the substructured frame, together with the identification of the mean value. | 21 |
| Figure 19. Comparison between the displacement recorded at the 2 nd story of the whole building (3D model) and those from the substructured frame for a) 75%, b) 100%, c) 125% and d) 150% of the selected record. | 22 |
| Figure 20. Different behaviour of alternative configurations for the infilled systems, namely single-squat infill wall (left), and rocking cantilever infill panels (right). | 23 |
| Figure 21. Disconnection of the infills from the surrounding frame. | 24 |
| Figure 22. Flowchart summarizing the main steps of the DBR procedure presented in D'Amore & Pampanin [20]. | 24 |
| Figure 23. Design process for timber-based exoskeletons. | 25 |
| Figure 24. Results of the non-linear static analyses for the infilled and bare frame system in the as-built configuration in terms of a) push-over, and b) inter-story drift ratio at the attainment of the LSLS. | 26 |
| Figure 25. Modelling approach for buildings retrofitted using the low-damage exoskeleton. | 27 |
| Figure 26. a) Results in terms of push-over curves for the as-built and retrofitted configuration, and b) results of cyclic non-linear static analysis (push-pull) to prove the self-centring capabilities of the external exoskeleton. | 27 |
| Figure 27. Geometric characteristics of the exoskeleton. Details 1 to 3 (i.e. Det. 1, Det. 2, and Det. 3) are presented in the following Fig. 28. | 28 |
| Figure 28. Details of the connection systems designed for the exoskeleton. | 28 |
| Figure 29. Comparison between the displacement recorded at the 2 nd story of the whole building (3D model) and those from the substructured frame for a) 75%, b) 100%, c) 125% and d) 150% of the selected record. | 29 |
| Figure 30. Dowelled Connection. | 30 |
| Figure 31. T-profile solution for connecting the exoskeleton to the as-built structure (left), and modification by fastening the timber beam from below, thus reducing potential architectural incompatibility (right). | 31 |
| Figure 32. Schematic representation of the bow-tie connection concept. e: eccentricity. | 32 |

LIST OF TABLES:

| | |
|--|----|
| Table 1. Modelling assumptions and considered parameters for hysteresis rules..... | 18 |
| Table 2. Selected earthquake record for NLTHAs. PGA: Peak Ground Acceleration in “g”, D: Epicentral Distance in “km”, Mw: Moment Magnitude, Soil Cl: Soil Class according to Eurocode..... | 20 |
| Table 3. Mechanical characteristics of the Glulam GL30C..... | 26 |

1. INTRODUCTION

The main scope of this deliverable is to discuss the experimental tests scheduled at the University of Naples Federico II (UNINA). The tests are intended to demonstrate the efficiency and effectiveness of the timber-based low-damage (implementing the Prestressed-Laminated, Pres-Lam, technology) exoskeleton solution proposed for the seismic retrofitting of existing Reinforced Concrete (RC) buildings.

One full-scale prototype has been developed to prove the high performance of the proposed solution through Pseudo-Dynamic (PsD) tests to reproduce seismic actions imposing equivalent displacement loading protocols. The prototype is characterised by a single-bay two-floor full-scale exoskeleton connected to a full-scale multi-story infilled RC frame, representative of typical existing RC buildings erected before the enforcement of modern seismic codes. The infilled RC frame system has thus been selected for being representative of typical existing buildings, including the Italian demo (Fig. 1) (i.e. the Acerra building demonstrator) where such a technology will be implemented for promoting the holistic (seismic-energetic-aesthetic) rehabilitation of the building.



Figure 1. The Acerra demonstrator from outside.

2. LOW-DAMAGE EXOSKELETON TECHNOLOGY

One of the most important goals of the MULTICARE project is the development of integrated solutions for enhancing the resilience of the built environment against multiple hazards (i.e., earthquakes, heat waves, floods, etc.). In this perspective, within Work-Stream 5 (WS5), an exoskeleton-based solution, facilitating holistic rehabilitation (seismic, energetic, architectural), was developed. More specifically, the exoskeleton is a newly designed structural system (both in the form of frame and wall systems) externally attached to the existing one. Such an additional structural system promotes seismic retrofit, thus increasing the strength and stiffness of the retrofitted building when compared to the as-built configuration. Moreover, such a newly designed structural system can support new multi- and high-performance “double-skin” facade systems, ultimately promoting energy refurbishment and architectural renovation, as schematically shown in Fig. 2a.

Additionally, another important point to stress is that such a renovation strategy exploits low-damage systems both for structural (exoskeleton) as well as for non-structural components (facade system). This aspect represents an important advancement concerning the current state-of-the-art. To better understand this aspect, it is worth mentioning the well-known performance matrix defined in the field of earthquake

engineering (Structural Engineers Association of California, SEAOC Vision 2000, [1]). Such a matrix defines different performances of the considered building, varying the earthquake intensity, as illustrated in Fig. 2. Consequently, the performance of existing buildings can be expected in the upper-right part of the matrix itself (shaded red area in Fig. 2b). Even though nowadays several strategies/techniques are available to enhance the seismic performance, thus achieving the “basic objective” (i.e., the diagonal of the matrix), it is easy to understand that in case of a “rare” or “very-rare” event (i.e., a strong earthquake), the extent of the damage could be too high, with associated unsustainable socio-economic losses. This consideration justifies the crucial need to move towards a damage-control approach in defining retrofit interventions and underlines how the MULTICARE project promotes an advancement with respect to the current state-of-the-art. Indeed, the MULTICARE project promotes the implementation of low-damage technologies to enhance the seismic performance of the built environment, which, considering the performance matrix, means moving towards the left part of the matrix itself (red line in Fig. 2b), ultimately enhancing the seismic resilience.

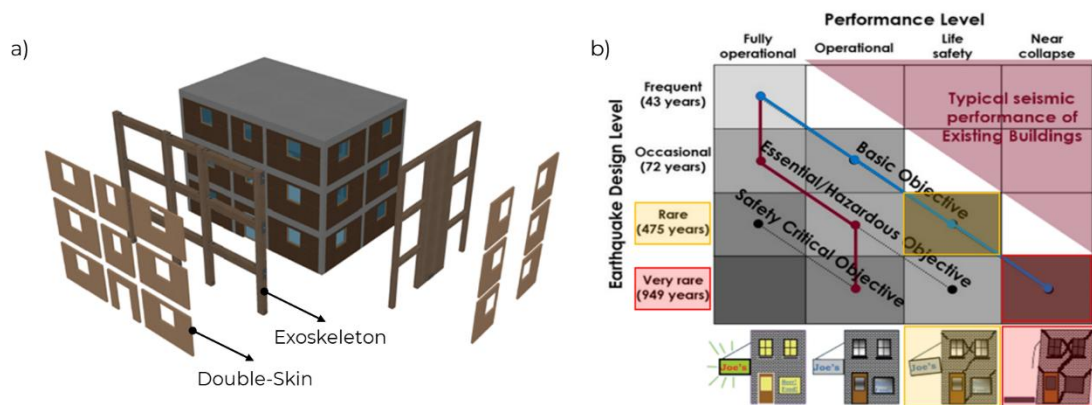


Figure 2. a) Schematic representation of the integrated rehabilitation based on low-damage timber-based exoskeletons, and b) seismic performance matrix with identification of the basic and enhanced design objective (modified after SEAOC [1] and Pampanin [2]).

Concerning the structural exoskeleton, which is the focus of this experimental campaign, the low-damage technology implemented is the Pres-Lam technology [3–5], which was proposed as the extension to timber of the PREcast Seismic Structural System (PRESSSS, [6–8]), developed in the 1990s at the University of California San Diego under the US PRESS programme for RC buildings. The Pres-Lam technology has been developed and tested over the past decades at the University of Canterbury [4] (Fig. 3a) and has already been implemented in New Zealand for the construction of resilient new buildings [9] (Fig. 3b).



Figure 3. a) Example of experimental test on a beam-column joint based on the Pres-Lam technology [4], and b) NMIT Arts & Media Building realized by implementing the Pres-Lam technology [9].

Adopting such a low-damage technology limits the damage in structural components by replacing the development of a plastic hinge with a controlled rocking and dissipative mechanism at the interface between structural components. The jointed ductile and dry connections of the system (e.g. beam-to-column, wall-to-foundation) feature two kinds of reinforcement: i) internal mild steel, or more recently (and preferably) external fuse-type Plug&Play dissipaters which ensure the dissipation capabilities of the system and are easily replaceable in case of a severe earthquake; and ii) an un-bonded cable, designed to remain elastic, which ensure the self-centering capabilities of the system at the end of the earthquake shaking, thus ensuring negligible/limited residual displacements. The adoption of such a technology allows for meeting design criteria related to the reduction of the expected losses and repair time. Indeed, in the case of the PRESSS or Pres-Lam technology, all of the operations related to the repair of the damage associated with plastic hinges development are replaced by the substitution of “Plug&Play” dissipaters. Moreover, the adoption of self-centring systems allows for considerably limiting the economic losses and loss of functionality related to residual displacement/drift, which are well recognized as an important damage parameter [10]. Fig. 4 illustrates an example of a jointed and ductile connection in the case of column-to-foundation connection (a), together with the peculiar hysteretic behaviour featuring the low-damage technology herein considered (b).

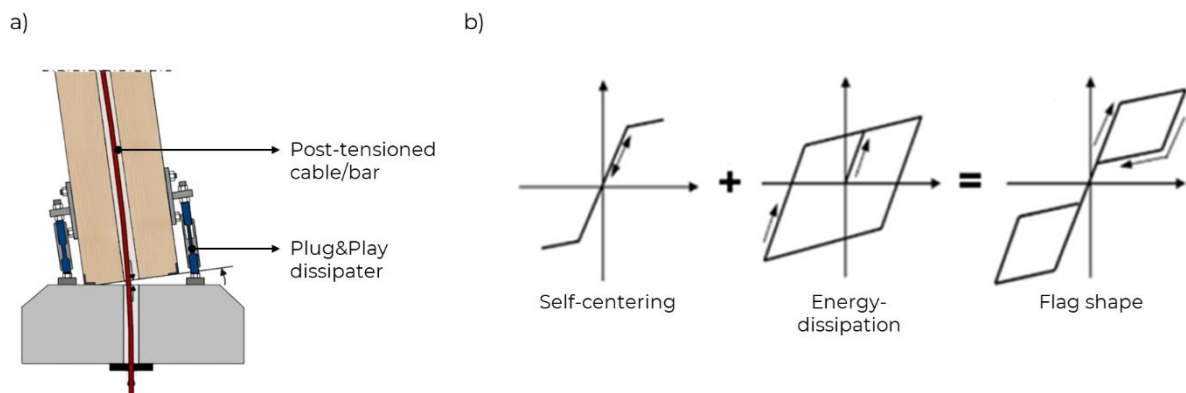


Figure 4. a) Example of a low-damage column-to-foundation connection, and b) hysteretic behaviour of the low-damage system considered (Pres-Lam), modified after fib [11].

3. EXPERIMENTAL TESTS

The retrofit solution proposed in Chapter 2 will be tested using the facilities available in the laboratories at the University of Napoli Federico II (UNINA). In agreement to the MULTICARE project, the exoskeleton will be applied on a full-scale one-bay two-storey infilled reinforced concrete (RC) frame specimen extracted from an existing building designed to sustain gravity load only (i.e., following a Gravity Load Design, GLD), selected as a case study to be assessed under pseudo-dynamic load. First, the selected frame will be tested in its “as-built” configuration to analyze the lateral response. In addition, the specimen will be damaged to achieve a proper damage state (DS) to be retrofitted. Then, the tests will be performed on the retrofitted frame to evaluate the contribution in terms of lateral stiffness and strength provided by the exoskeleton to the existing RC frame.

3.1 Facilities of UNINA Laboratories

The University of Study of Naples Federico II owns two laboratories dedicated to structural assessment. The first is the laboratory of the Department of Structures for Engineering and Architecture (DiST), located in the western area of Naples (see Fig. 5). It is equipped with

facilities that allow performing the structural assessment of different systems using the following testing methods:

- Static tests.
- Dynamic tests.

The static testing method is used to assess the response of structural components as:

- Columns
- Beams
- Beam-Column Joints (BCJ)
- Single-story full-scale infilled (or not) RC frame
- Framed structures

As well as the response of non-structural components:

- Infills
- Light-Partitions

The response of these components can be assessed under different loads:

- Horizontal load (uniaxial or biaxial direction).
- Compression load.
- In-plane and out-of-plane (walls).
- Flexural (columns and BCJ).



Figure 5. Overview of the DiST laboratory and available facilities.

The dynamic response of structural systems is assessed with two shaking tables available in the laboratory, as shown in Fig. 6. The system consists of two 3 m x 3 m square shake tables. Each table is featured by two degrees of freedom in the two horizontal directions acting in both synchronous and asynchronous manner. The maximum payload of each shake table is 20 tons with a bandwidth of 0–50 Hz, acceleration peak equal to 1.0g, and total displacement equal to 500 mm (± 250 mm).

The second laboratory was built in the *Centro Servizi Metrologici e Tecnologici Avanzati* (CeSMA), in the eastern part of the city, and it is managed by the Department of Structures for Engineering and Architecture (DiST). In this laboratory, an RC strong wall and floor were realized. It has been recently equipped with a PsD testing framework with the specific purpose of testing full-scale multi-story infilled RC frames in different configurations (i.e., as-built or retrofitted).



Figure 6. Shaking tables available at DiST laboratory.

The rising attention of the research community to such a type of test is related to the simplicity of the seismic testing of full-scale specimens without using complex and expensive dynamic facilities, with the main advantage of overcoming the limitations related to the quasi-static predefined loading protocols and shaking table payload. The details of the laboratory and the implemented PsD testing framework are presented in the next section.

3.1 Pseudo-Dynamic Tests

The response of the proposed retrofit solution applied to the full-scale (two-story one-bay) infilled RC frame will be tested under pseudo-dynamic load using the infrastructure of the Laboratory of Testing on Real Scale Structures (LaSTRUT) at the University of Naples Federico II (Fig. 7).



Figure 7. Overview of the CeSMA laboratory and available facilities.

It is an indoor laboratory with a reaction wall 7.0 m high, 12.0 m wide and 1.80 m thick, and a 260 m² strong floor served by a crane of 10 tons lifting capacity. An anchor hole grid is realized both on the wall and the strong floor to allow the installation of the testing set-up (e.g., steel plates, hydraulic jacks, frames).

The laboratory is equipped with four hydraulic actuators with a capacity of 1200 kN (in tension and compression) and a total stroke of 750 mm, and two hollow jacks with a capacity of 750 kN and a total stroke of 300 mm, both served by a hydraulic pump system. Within this testing program, only two hydraulic jacks will be used to apply the in-plane (IP) displacement at the first and second storey of the specimen. The out-of-plane (OOP) actions will not be simulated during the tests. The two hollow jacks will be positioned at the top of each column to apply the vertical load constantly during the tests. The definition of the vertical loads, which will be applied to the specimen, is discussed in Chapter 5. The tests will be performed in displacement control recording the feedback by using two high-precision displacement transducers installed at each storey at the centre of the beam in agreement with the nonlinear models developed for the numerical simulations.

The PsD framework implemented in the laboratory (see Fig. 8), with the specific purpose of testing full-scale multi-storey infilled RC frames, will be used to test the response of the as-built and retrofitted specimens. The framework consists of a Coordinator System (A), a Control System (B), the test specimen (C), and a data acquisition system (D).

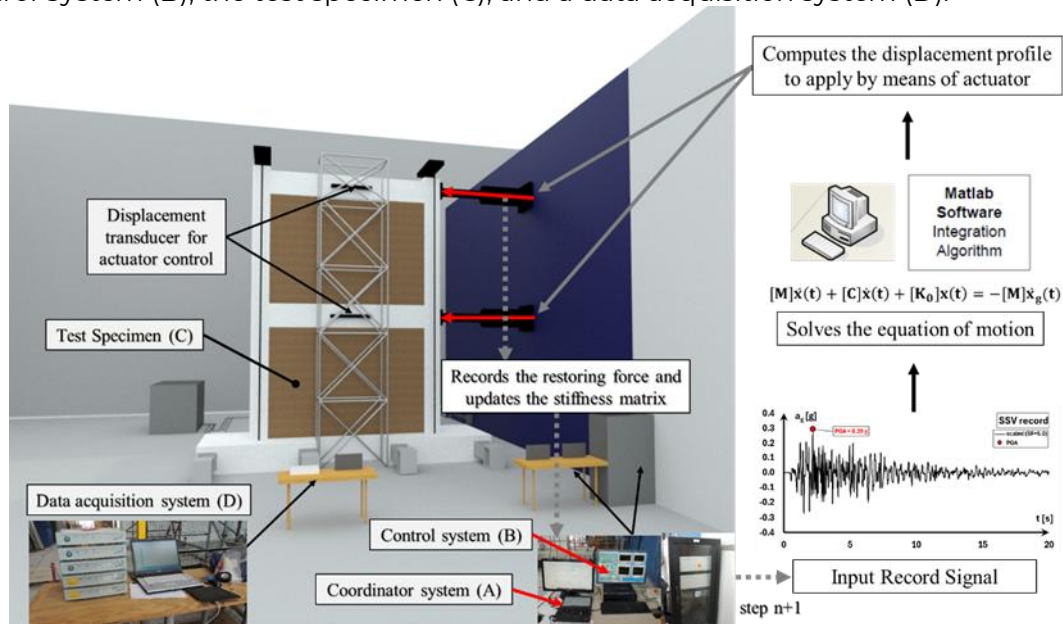


Figure 8. Pseudo-dynamic testing procedure.

The coordinator system (A) consists of an input suite, the numerical solver of the equation of motion, a communication suite with the control system (B), and a real-time output interface. The dynamic properties of the specimen must be defined in the input suite. The control system (B) consists of the controller and a personal computer. It allows for managing input/output, the system configurations, and the data recorded during the tests by means of a real-time graphical user interface. A Hardware-in-the-loop (HIL) interface has been developed in the controller to communicate with the coordinator system (A) for the specific purpose of conducting PsD tests. A data acquisition system (D) will be used to record data from the instrumentation which will be installed on the specimen. High-precision Linear Variable Displacement Transducers LVDTs, classic LVDTs, strain gauges, and potentiometers will be used to monitor global and local deformations as well as strain on internal reinforcements.

The testing procedure adopted to carry out the tests is also shown in Fig. 8. It requires the definition of an input record signal and the relative time step integration, dt , the matrix of masses $[M]$, and initial stiffness $[K]$. The mass matrix $[M]$ of the specimens is numerically evaluated by using a simplified substructuring approach. This approach is presented in Chapter 5. The stiffness matrix $[K]$ is defined based on experimental measurements of the reaction force under a low-magnitude displacement profile in both directions (pushing and pulling). The input record signal which will be used to carry out the PsD tests is selected according to the site of the case study building. The criterion adopted to select the input record signal is discussed in Chapter 5. The equation of motion will be solved at each time step by using an implicit integration method. The computed displacement profile will be applied to the specimen, and the recorded displacements and the restoring forces at each level will be recorded using high-precision transducers and load cells. The recorded measures will be used by the coordinator system to update the stiffness matrix before moving to the following step of the record. This will allow the reproduction of the actual displacement demand of the earthquake by considering the strength and stiffness degradation that is significant in existing infilled RC buildings.

4. CASE-STUDY BUILDING FOR PSEUDO-DYNAMIC TESTS

The case study building herein considered is an archetype building derived from the information available from the “Bonefro Building” (Fig. 9), an Italian building quite “famous” in the scientific literature, which was damaged by the “San Giuliano di Puglia Earthquake” in 2002 [12]. The present case study is for residential use and is located in Bonefro. The case study is a four-story RC-infilled frame building with a plan of 19.50 m x 10.05 m, and an inter-story height equal to 3.10 m. Concerning the structural system, the building presents three Moment-Resisting Frames (MRF) in the longitudinal direction (the two perimetral frames have deep beams, while the central one features hidden beams), and four MRFs in the transversal one (two perimetral frames with deep beams, while the others have hidden beams).

The building has been designed for gravity loads only and by following a “working stress” approach, thus lacking any considerations related to “capacity design” and “hierarchy of strengths” as imposed by modern seismic codes. Consequently, the building is expected to reflect the typical deficiencies/vulnerabilities of buildings erected in the pre-code era, and thus it is expected to be “potentially” seismic-prone.

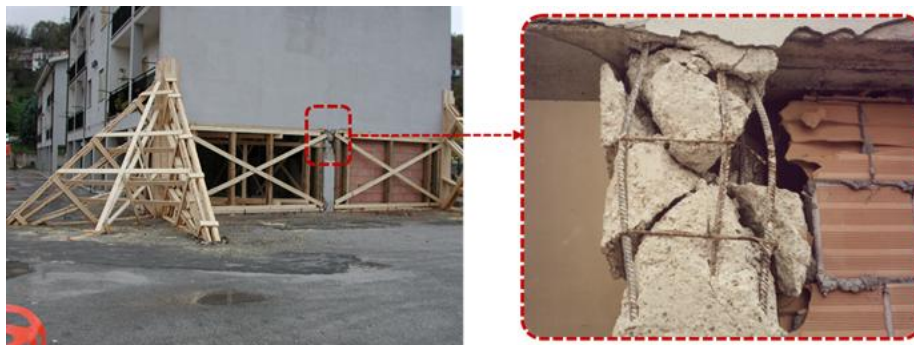


Figure 9. Bonefro building damaged during the San Giuliano di Puglia Earthquake (left), with identification of a brittle shear failure in the RC column due to interaction between the RC frame and the masonry infills, modified after [12].

Fig. 10 illustrates the geometric characteristics of the considered building in terms of plan view and lateral view. Concerning mechanical properties of materials, concrete has a compressive strength equal to 20 MPa, with a peak (ε'_c) and ultimate strain (ε_{cu}) equal to 0.0020 and 0.0035, respectively. Concerning reinforcing steel, in line with the properties of deformed bars realized using FeB44k, the yielding (f'_y) and ultimate (f'_u) stress have been considered equal to 430 MPa and 210 MPa, respectively, while the ultimate strain (ε_{su}) has been set equal to 0.004 in line with the prescriptions of the Italian Building Code [13].

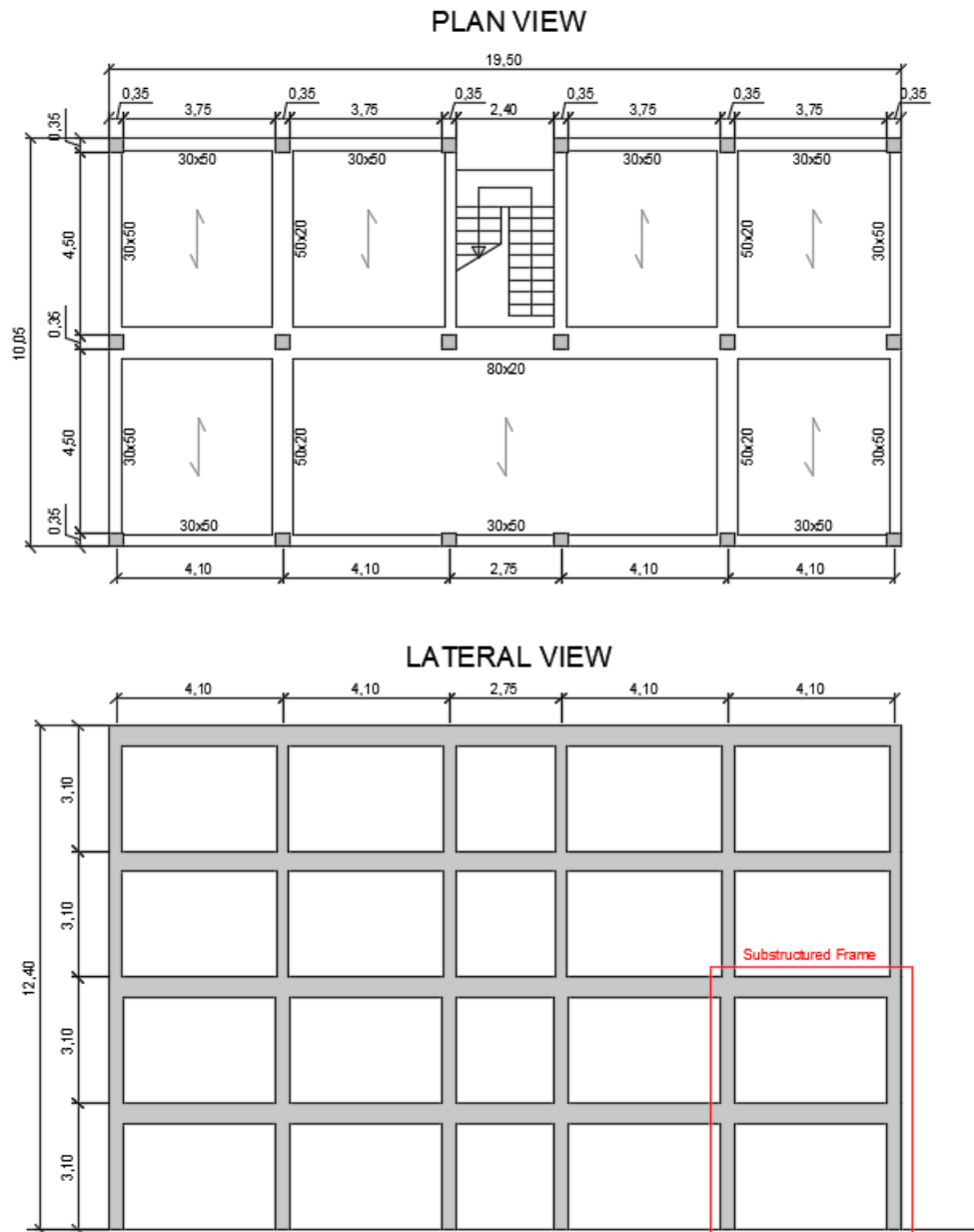


Figure 10. Geometric characteristics of the considered building in terms of plan and lateral view, together with the identification of the substructured frame.

Starting from this case study, the reduced portion (2-story, 1-bay frame) highlighted in Fig.10, has been selected for the experimental test. Further details related to the specimen are provided in the following section.

4.1 Test set-up for Pseudo-Dynamic Tests (As-Built configuration)

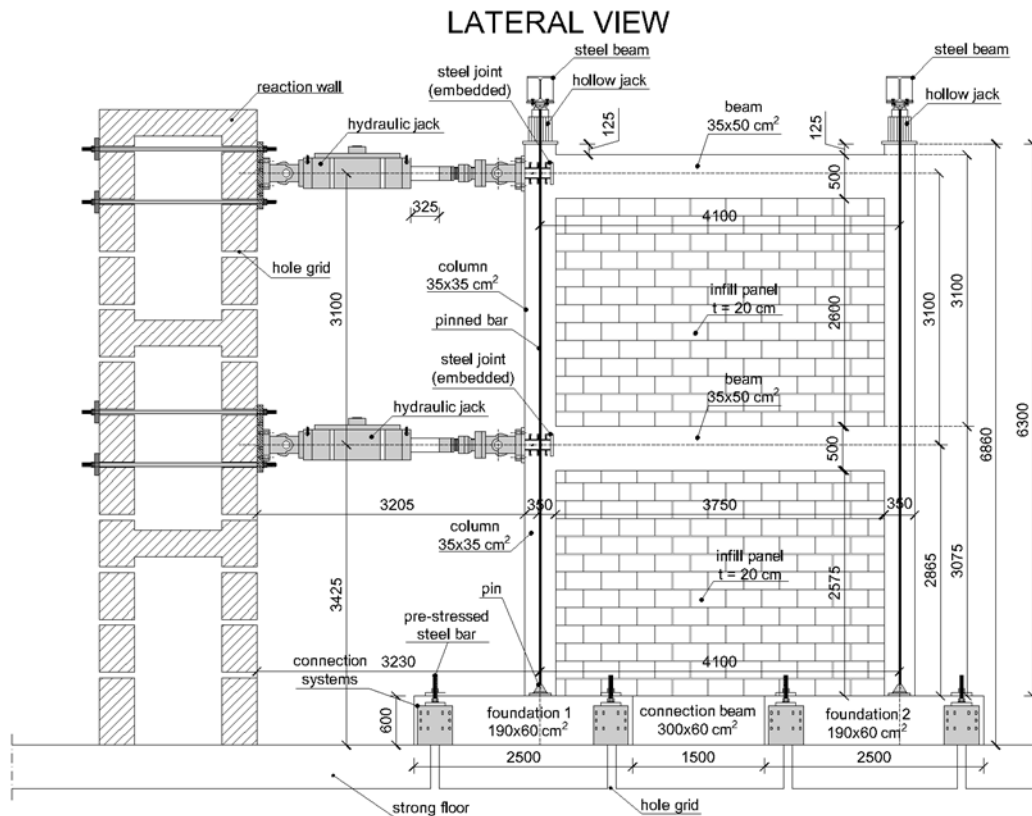


Figure 11. Test set-up: Front view.

The test set-up designed and realized to perform PsD test is reported in Fig. 11 and Fig.12. The frame will be constructed on a 0.60 m thick RC foundation clamped to the strong floor by means of pre-stressed steel bars. Eight additional steel profiles with a portion embedded in the foundation block will be used to avoid horizontal sliding. The additional profiles are also clamped to the strong floor using pre-stressed steel bars. The frame is connected to the actuators through steel profiles embedded in the left beam-column joints. Once the frame is realized, the jacks will be positioned at the top end of the columns. During the tests, the jacks will be contrasted on the steel beam linked to the specimen foundation using two pinned bars to apply the vertical load.

The specimen will be 6.30 m high and 4.45 m wide. The interstorey height will be equal to 3.10 m while the distance between the centroid axis of the columns will be 4.10 m. The columns will have a square cross-section with 350 mm sides, while the beams will be 500 mm high and 350 mm wide. The members will have the same cross-section on both stories. The infill panels will have a clear height of 2.57 m and a clear length of 3.75 m. The panels will be made of hollow clay bricks 200 mm thick with holes parallel to the direction of loading (horizontal holes) and connected to the surrounding frame on four sides with mortar, as is generally done in common practice.

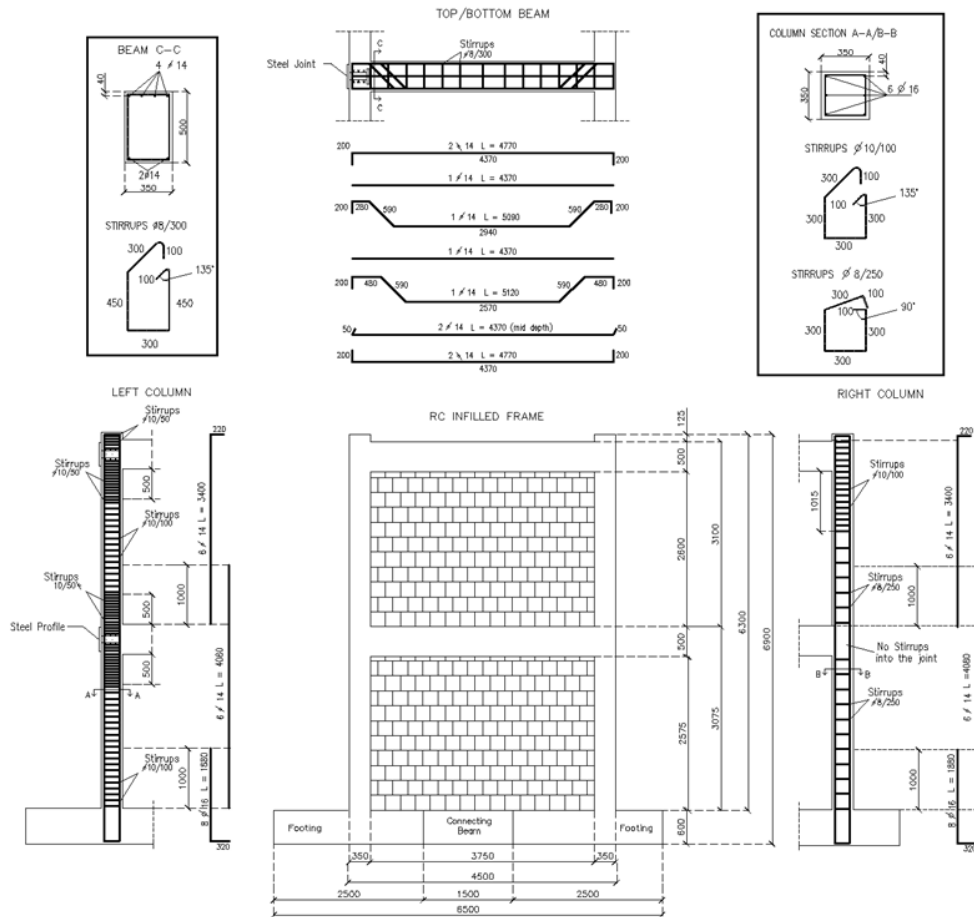


Figure 13. RC frame geometry and reinforcement details.

At this stage, the parts of the test set-up are ready for the installation. The casting of the concrete frame is also currently ongoing.

5. NUMERICAL SIMULATIONS FOR THE AS-BUILT CONFIGURATION

This chapter presents the results of all the numerical simulations that have been carried out before the tests that will start soon at the laboratory of the University of Naples Federico II. Firstly, a description of the modelling approach adopted to perform seismic analyses in the as-built configuration is presented. After this, the procedure adopted to define the record used for Non-Linear Time-History Analyses (NLTHA) is presented. Finally, the results of NLTHAs carried out to validate the substructuring approach adopted for this experimental campaign are discussed.

5.1 Modelling Approach for the As-Built configuration

Numerical models have been implemented in the software SAP2000 for Finite Element Modelling (FEM) [14]. More specifically, a lumped plasticity approach has been adopted, and mono-dimensional frame elements with plastic hinges at the end sections have been used for modelling structural components. Both for beams and columns, the plastic hinges' behaviour is modelled through moment-curvature relationships, and the plastic hinges'

length is defined according to Priestley et al. [15]. The shear and shear/flexure failures have also been considered by following the instructions of the New Zealand Society of Earthquake Engineering (NZSEE) guidelines for seismic assessment of existing buildings [16]. Concerning the hysteretic behaviour, as in the case of past research works (e.g., Moliterno et al. [17]), the Pivot model available in SAP2000 has been adopted, and the parameters adopted can be found in Table 1.

| Member | Non-linear Element | Hysteresis Model | Parameters |
|-----------------------------|---|------------------|---|
| Columns | Frame with plastic hinges at the end sections | Pivot | $\alpha_1=10$ $\alpha_2=10$ $\beta_1=1$ $\beta_2=1$ $\eta=0.8$ |
| Beams | Frame with plastic hinges at the end sections | Pivot | $\alpha_1=10$ $\alpha_2=10$ $\beta_1=1$ $\beta_2=1$ $\eta=0.9$ |
| External Beam-Column Joints | Rotational Springs | Pivot | $\alpha_1=1$ $\alpha_2=1$ $\beta_1=0.15$ $\beta_2=0.15$ $\eta=0.8$ |
| Internal Beam-Column Joints | Rotational Springs | Pivot | $\alpha_1=0.5$ $\alpha_2=0.5$ $\beta_1=0.15$ $\beta_2=0.15$ $\eta=0.8$ |
| Infills | Axial Spring (compression only) | Pivot | $\alpha_1=0$ $\alpha_2=0.25$ $\beta_1=0$ $\beta_2=0$ $\eta=0$ |

Table 1. Modelling assumptions and considered parameters for hysteresis rules.

Beam-column joints have been modelled by using a system of rigid links and rotational springs. The moment-shear deformation relationship has been defined by following the instructions available in [16]. As in the case of beams and columns, the hysteretic behaviour has been modelled using the Pivot model. Here, the parameters of the pivot have been defined by replicating in SAP2000 beam column joints tested in past research activities [18]. The results of such a calibration are shown in Fig. 14 for external T-joints (left) and internal joints (right). The derived parameters for the Pivot model are provided in Table 11.

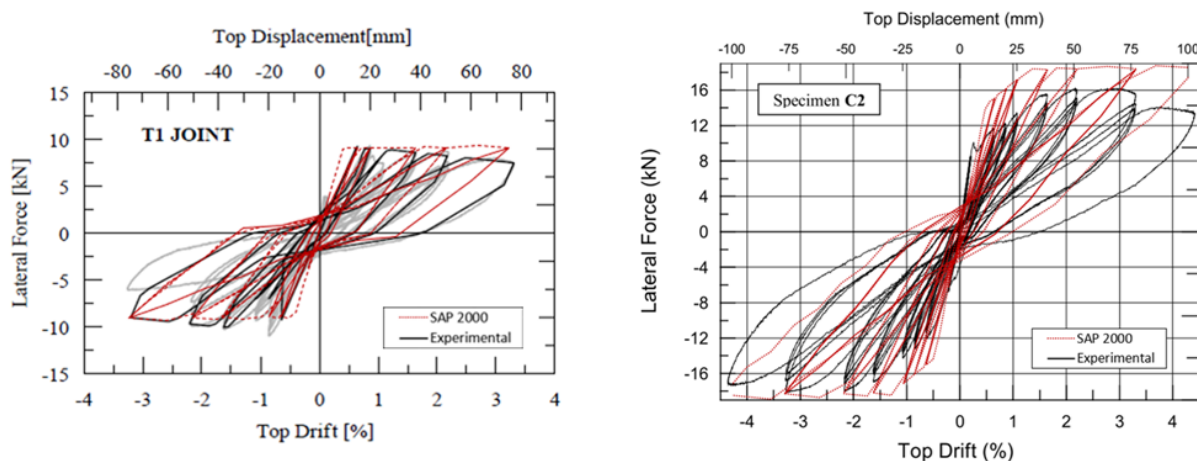


Figure 14. Results of the calibration of the Pivot hysteresis model parameters for an external beam-column joint (left), and for an internal one (right). Modified after Pampanin et al. [18].

Concerning masonry infills, a single strut model has been considered. Each infill panel has been modelled using two links working only in compression. The shear-displacement relationship proposed by Panagiotakos & Fardis [19] has been adopted to model the response of the infill. A tri-linear force-displacement relationship considering the cracking, peak, and residual strength has been derived for each infill panel. The hysteretic behaviour, as in the previous cases, has been modelled by using the Pivot model. The Pivot parameters

adopted (available in Table 1) have been defined according to Moliterno et al. [17], who defined such parameters according to the results of previous experimental tests on infilled frame RC systems.

Finally, for the sake of simplicity, soil-structure interaction has been neglected, and fixed-base connections have been assumed. A schematic representation of the adopted modelling approach is provided in Fig. 15.

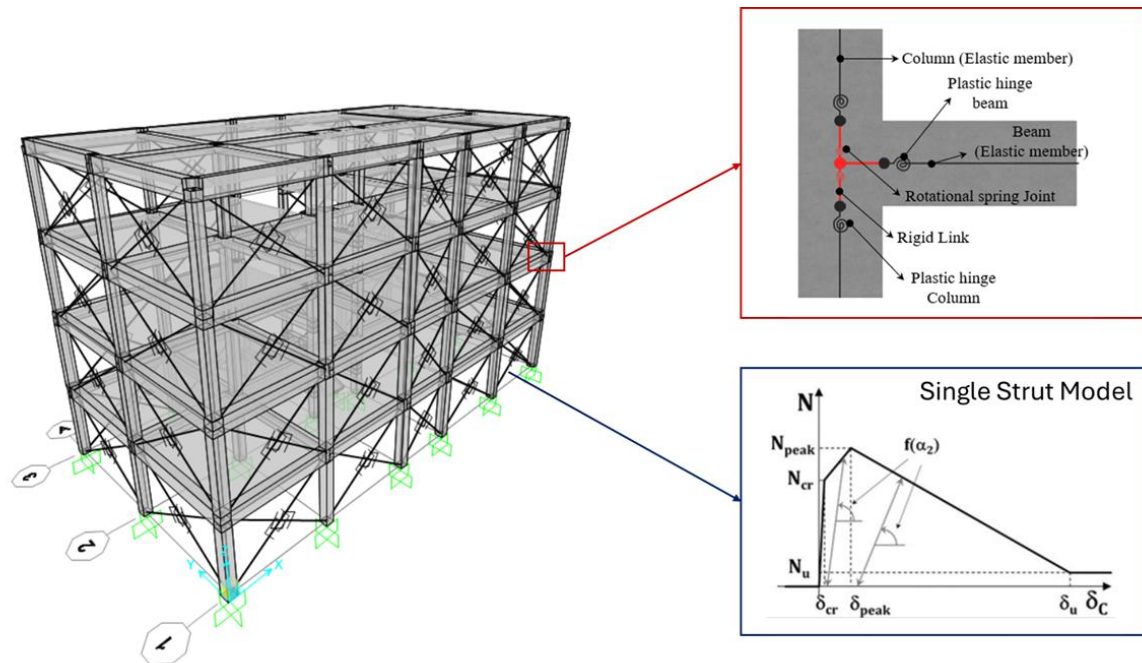


Figure 15. Modelling approach for existing RC infilled frame buildings. Modified after Moliterno et al. [17] and D'Amore & Pampanin [20].

Both non-linear static and NLTHAs have been performed neglecting the second-order effects (i.e., the P- Δ effects). Such a choice is justified by the relatively limited drift demand and considering the relatively reduced height of the building (i.e. 4-story building). For non-linear static analyses, a load distribution proportional to the story masses has been considered, while for NLTHAs, the Rayleigh damping coefficients are determined by imposing a 2% damping value at the first two vibrational modes in the direction of interest (i.e., longitudinal direction).

5.2 Selection of the record for NLTHAs

In order to carry out both NLTHAs and the PsD experimental tests, the definition of a record was needed. Considering that the selected record must be representative of the seismicity of the site (i.e., Bonefro), the recommendation of the Italian Building Code [13] have been followed to define a suite of seven natural (i.e., unscaled) records spectrum-compatible with the Life-Safety Limit-State LSLS (probability of exceedance equal to 10% in 50 years, corresponding to a return period $T_R=475$ years) spectrum for the city of Bonefro. To define the LSLS spectrum, a soil class C, according to the Italian Building Code [13] was considered. The resulting Peak Ground Acceleration (PGA) is equal to 0.290g. The online tool "RexelWeb" [21] was used to define the suite of seven unscaled records. More specifically, this tool allows for defining such natural records having magnitude and fault distance, which are consistent with the specific site considered. Fig. 16a presents the spectra of the seven records, compared with the LSLS spectrum of Bonefro. Moreover, the spectrum of the record selected among the seven is highlighted (red line). Such an event has been

selected since it is the one with the PGA and spectral shape (in the period range of interest) most similar to the code spectrum. Fig. 16b presents the accelerogram of the event, while Table 2 summarizes the crucial information of the record itself.

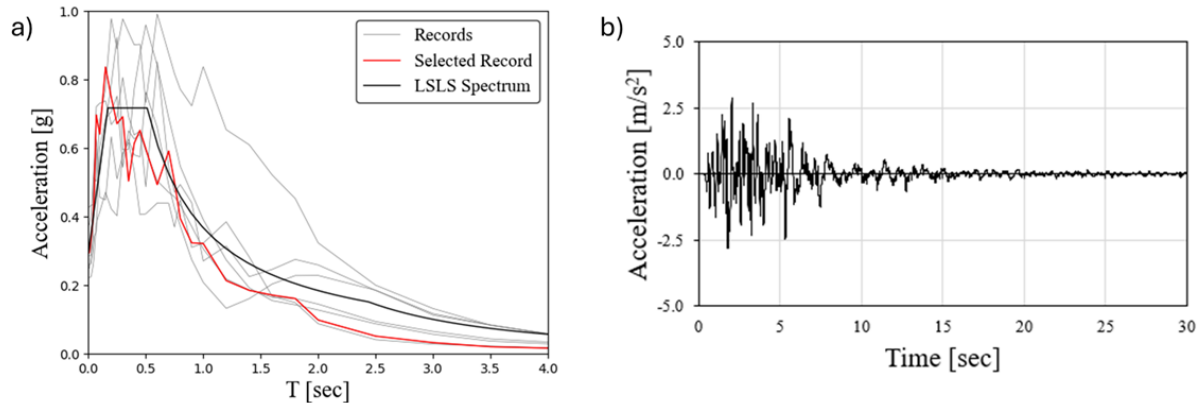


Figure 16. a) Spectrum of the selected record (red) compared with the other spectra from the spectrum-compatibility procedure (gray) and the code-spectrum for the city of Bonifro at LSLs, and b) accelerogram of the selected record.

| Earthquake | Station Code | Event ID | PGA [g] | D [km] | Mw | Soil Cl |
|--|--------------|-----------------------|---------|--------|-----|---------|
| Central Italy sequence. 30-Oct-2016 | CNE | EMSC-20161030_0000029 | 0.294 | 6.7 | 6.6 | C |

Table 2. Selected earthquake record for NLTHAs. PGA: Peak Ground Acceleration in “g”, D: Epicentral Distance in “km”, Mw: Moment Magnitude, Soil Cl: Soil Class according to Eurocode.

5.3 Substructuring approach and results from NLTHAs

Considering the physical limitation in the height of the laboratory, and in order to avoid scaling the specimen, only a full-scale two-story one-bay infilled frame has been selected for reproduction in the laboratory. The frame is a perimetral frame with a corner column. Further information related to the test set-up has already been provided in §4.1.

The PsD testing procedure requires as input the definition of both the mass and the initial stiffness matrix, as well as the rules for combining the different floor stiffnesses for assembling the initial stiffness matrix. For this reason, a detailed analysis of mass and stiffness distribution is performed by using the previously discussed numerical model of the whole building, as well as a reduced model representing the specimen to be tested in the laboratory. The stiffness matrix is defined based on experimental measurements of the reaction force under a low-magnitude displacement profile in both directions (pushing and pulling). The mass matrix is defined with a simplified substructuring approach proposed in [17]. It is a stiffness-based which relies on both the results of a modal analysis as well as on the results of the non-linear static (push-over) analyses performed on the numerical models mentioned before. This approach has been verified by comparing the results of NLTHAs at both the global (whole building) as well as at the local one (substructured frame).

At first, a modal analysis has been performed considering the initial stiffness of both structural and non-structural (i.e., infills) elements. The result of such analysis shows that in the direction of interest (i.e., longitudinal, or X-Direction) the participating mass at the first mode is considerably higher (82%) when compared to higher modes, as illustrated in Fig. 17.

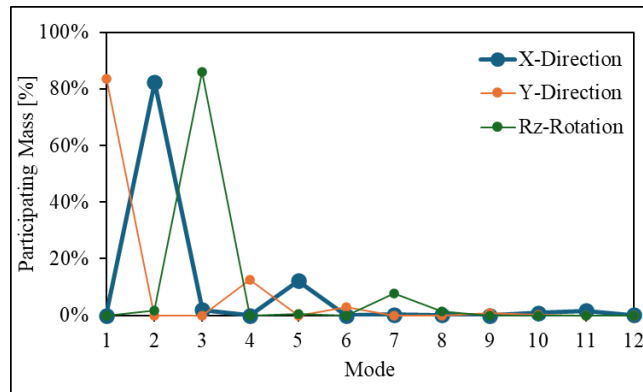


Figure 17. Modal participating mass from the modal analysis of the numerical model of the whole building.

Consequently, it can be stated that the seismic response of the building can be well approximated through a push-over analysis with displacement applied in the same direction. Building on this important assumption, the lateral response of both the building and the substructured frame has been defined using push-over analyses. More specifically, several pushover analyses have been performed by applying a unitary force to a selected floor while restraining the others. The results of such analyses are presented in Fig. 18a. Then, the mass matrix is defined by considering the seismic forces effectively carried by the substructured frame, which can be easily defined through the push-over analyses mentioned before. More specifically, the floor mass m_i^* attributed to the substructured frame is the product of the total floor mass (i.e., $m_{i,Total}$ related to the entire building) and a coefficient representative of the ratio between the stiffness of the frame (K_{Frame}) and that of the whole building ($K_{Building}$). Such a coefficient, representative of the stiffness ratio, was defined by considering the variation of the ratio itself in a range of lateral displacement representative of the lateral response of the structures (Fig. 18b). After evaluating such a variation, a mean value was selected to define the m_i^* values, which in the specific case are equal to 20 Tons at the first story, and to 59 Tons at the second story. It is worth mentioning that the higher value applied on the second story of the substructured frame is justified by the fact that also the masses from the 3rd and 4th story (which are not modelled in the laboratory) are lumped here to be representative of the masses of the higher stories.

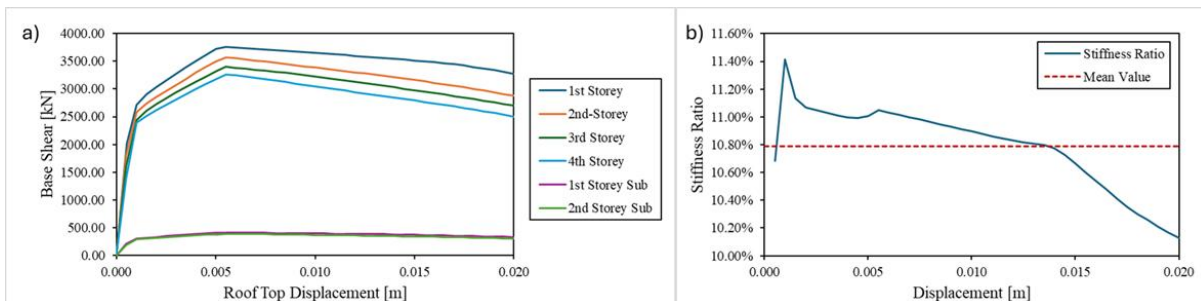


Figure 18. a) Floor push-over curves obtained both for the whole building as well as for the substructured frame, and b) ratio between the stiffness of the whole building and that of the substructured frame, together with the identification of the mean value.

Finally, the validation of the substructuring approach is carried out by comparing the results in terms of displacement at the 2nd story derived by the NLTHAs carried out on both the numerical model of the whole building and that of the substructured frame by using the selected input record signal described in the previous section §5.2. NLTHAs have been implemented using the record defined in §5.2 as input. Several NLTHAs have been carried out. Indeed, in addition to the selected record, this one has been scaled down to 10%, 25%,

50%, and 75%, and scaled up to 125% and 150%. A good match has been observed for all the considered intensities, as can be observed in Fig. 19 for the results of the analyses using the a) 75%, b) 100%, c) 125%, and d) 150% of the selected record. Although some differences in peak displacements can be observed, they are negligible with respect to the maximum displacements achieved, and the discrepancies tend to reduce while passing from 75% to 150%, where almost a perfect overlapping can be highlighted, thus confirming the reliability of the substructuring approach here considered.

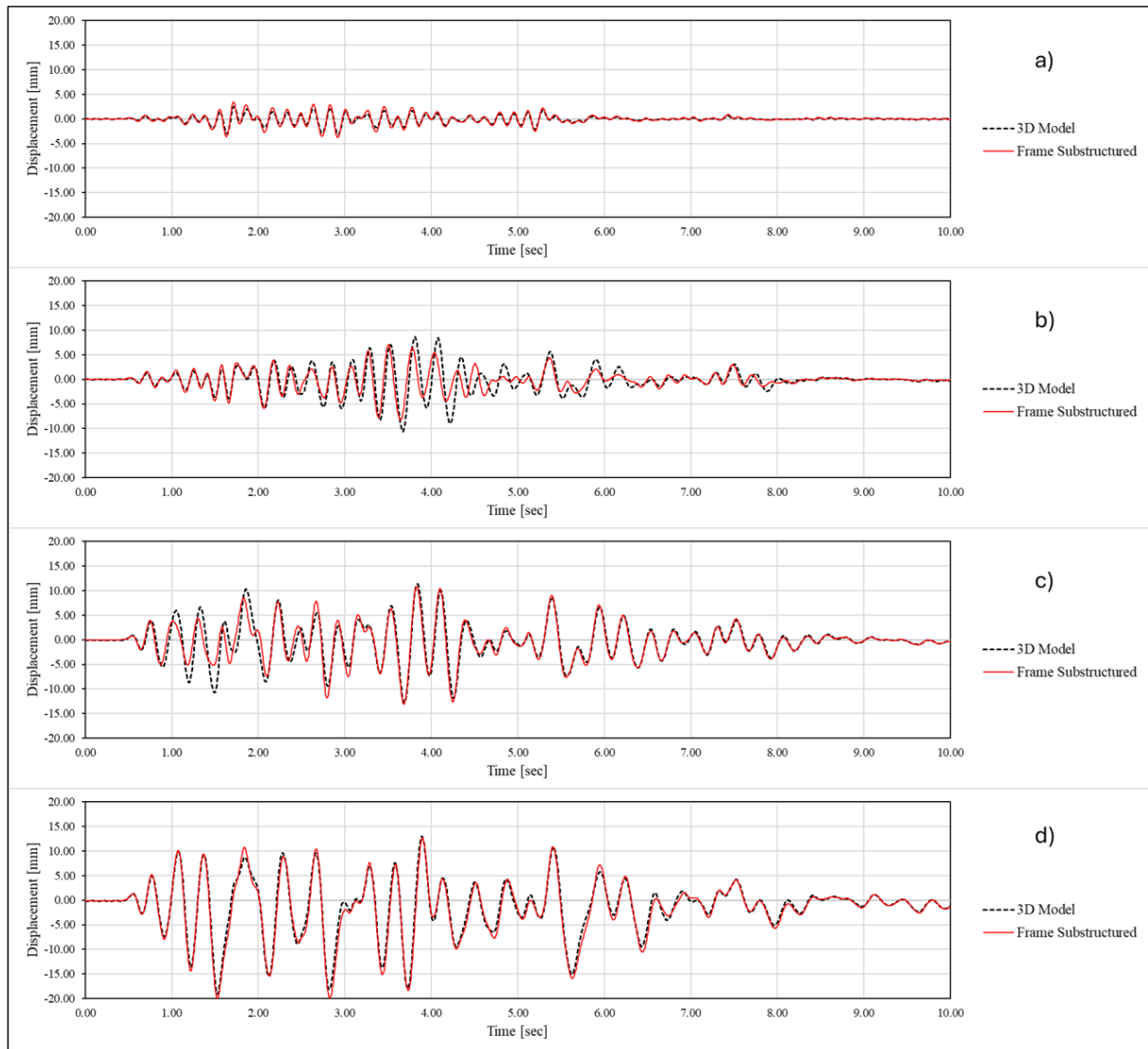


Figure 19. Comparison between the displacement recorded at the 2nd story of the whole building (3D model) and those from the substructured frame for a) 75%, b) 100%, c) 125% and d) 150% of the selected record.

Concerning these analyses, it is worth stressing that the models developed to prove the efficiency of the substructuring approach did not consider the effects of potential shear failures in structural members due to the interaction with masonry infills (e.g., the reader can consider as an example the shear failure presented in Fig. 9). Nevertheless, such a failure has been generally observed in experimental tests on RC infilled frames representative of existing buildings [17,22]. For this reason, more refined models (e.g., using a 3-struts approach for modelling infills) are currently under development to catch such an aspect. This will be crucial in the experimental campaign in order to predict the maximum

intensity that the specimen can withstand in the laboratory and to interrupt the experiments at the triggering of the shear cracking. This will ensure safety during tests and prevent brittle local failure, potentially causing the global collapse of the specimen. For this reason, even though the analyses have been carried out until 150% of the selected record, it is expected that the experimental campaign on the as-built specimen will be interrupted at lower intensities, also reflecting the expected typical vulnerabilities of existing GLD pre-code buildings.

6. METHODS FOR SEISMIC DESIGN OF THE LOW-DAMAGE EXOSKELETON

The main objective of this chapter is to present the technological implementation of the low-damage timber-based exoskeleton, while also providing information related to the displacement-based approach proposed to support the design procedure.

In any case, before the implementation of the structural exoskeleton, considering the remarked vulnerability of masonry infills, and aligning with the objective of moving towards a low-damage building system holistically, strategies emphasizing the implementation of low-damage technologies have also been proposed for enhancing the seismic performance of existing vertical envelopes (i.e., infills). This aspect is crucial, especially considering the high investment related to such elements within the building [23]. Furthermore, even in the case of a frequent level of shaking (i.e., low-to-moderate intensity earthquake), it is possible to note damage, almost entirely related to non-structural components [24]. Considering the reasons mentioned above, this research intends to provide an enhanced resilient solution that implements low-damage technologies both for the structural skeleton (i.e., for the exoskeleton) as well as for non-structural components (i.e., both for the retrofit of existing envelopes components, as well as for the installation of “double skin” facade systems supporting energy refurbishment and architectural renovation).

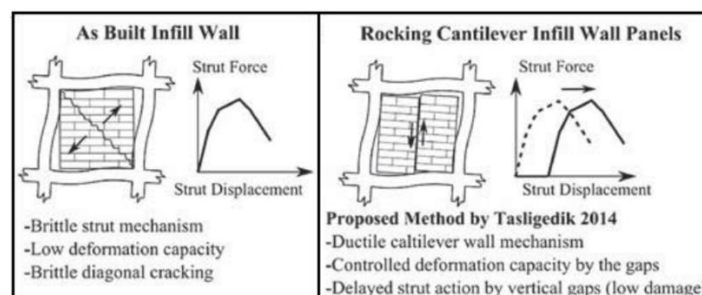


Figure 20. Different behaviour of alternative configurations for the infilled systems, namely single-squat infill wall (left), and rocking cantilever infill panels (right).

For enhancing the seismic resilience of existing infills, the in-plane seismic capacity is improved by disconnecting the monolithic panel from the surrounding RC frame, operating vertical and horizontal cuts, resulting in the introduction of lateral gaps. This operation turns the behaviour of a shear-dominated single-squat panel (potentially experiencing brittle failures) into a system consisting of discrete rocking clay brick infill wall panels capable of sustaining a high level of drift before incurring damage. As illustrated in Fig. 20, such a capability of experiencing a high level of drift is mostly related to delaying the development of the strut into the panel, which can develop only when the lateral gaps

get closed due to in-plane movement. Moreover, adopting this selective weakening approach on the masonry infills allows for preventing potentially critical shear failure on structural members triggered by the interaction between structural and non-structural components (see Fig. 9).

Further information related to this approach for enhancing the seismic performance of infill walls can be found in Tasligedik & Pampanin [25], who also demonstrated the efficiency of the system through experimental tests carried out at the University of Canterbury, New Zealand. Moreover, it is worth stressing that the possibility of implementing such an approach from outside the building, thus considerably limiting the owners' disruption, has also been proved by Preti & Bolis [26]. Fig. 21 illustrates a schematic representation of the intervention on existing infill panels.

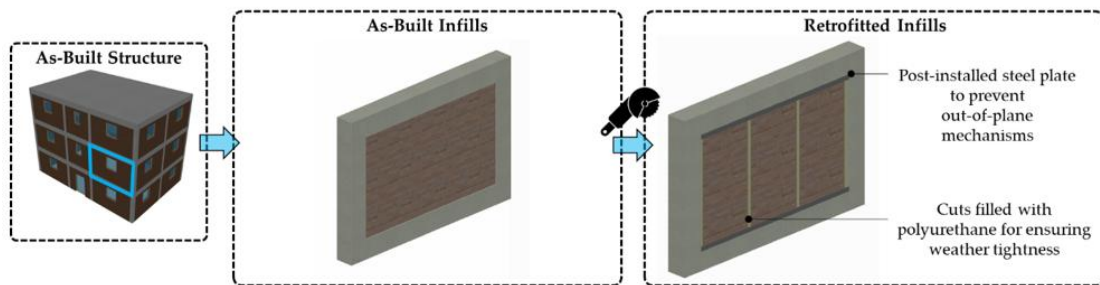


Figure 21. Disconnection of the infills from the surrounding frame.

Once this operation for enhancing the seismic performance of existing infills has been carried out, it is possible to install the low-damage exoskeleton based on the Pres-Lam technology (detailed information on Pres-Lam has been provided before in §2).

The exoskeleton has been designed by following the Displacement-Based Retrofit (DBR) proposed by D'Amore & Pampanin [20] for frame-type exoskeletons. The DBR procedure is a natural extension of the Direct-Displacement Based Design (DDBD) proposed by Priestley et al. [15,27,28] for the design of new structures. The main goal of the procedure is to prevent the existing structure from reaching and exceeding its failure displacement profile. The first step is to select a design drift or displacement that is defined through the assessment procedure carried out on the as-built structure. After this, the procedure (schematically shown in the flowchart in Fig. 22) can be applied to define the design base shear that the exoskeleton must withstand.

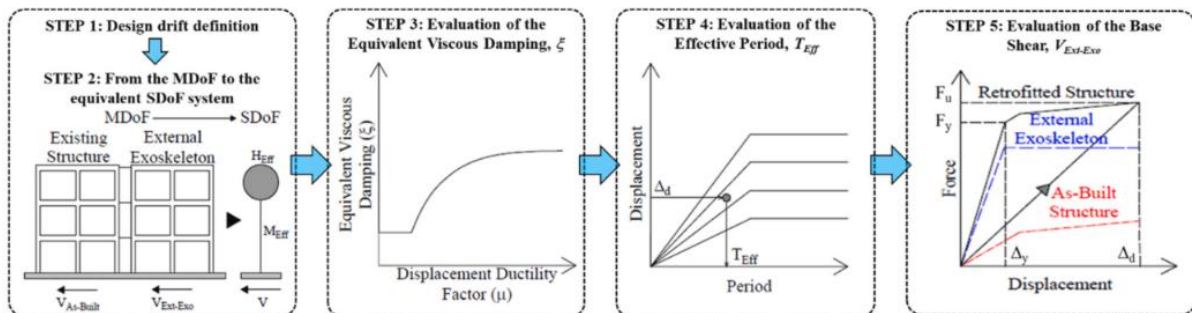


Figure 22. Flowchart summarizing the main steps of the DBR procedure presented in D'Amore & Pampanin [20].

Once the base shear at the LSLS has been defined, this can be distributed along the height of the building, and the internal actions can be easily defined using an equilibrium

approach. Finally, such internal actions can be used to design and detail all the connection systems of the exoskeleton itself.

In any case, it is worth stressing that in the case of timber-based exoskeletons, the procedure outlined before (presented for RC exoskeletons) should be slightly adjusted [29]. More specifically, when dealing with timber structures, the Damage-Control Limit-State (DCLS) generally governs the size of structural components and the amount of post-tensioning. Indeed, considering the higher flexibility of timber, it is crucial to provide adequate stiffness to prevent damage in the case of low-to-moderate (i.e., frequent) earthquakes. In other words, when dealing with timber structures, two steps are required, as shown in Fig. 23:

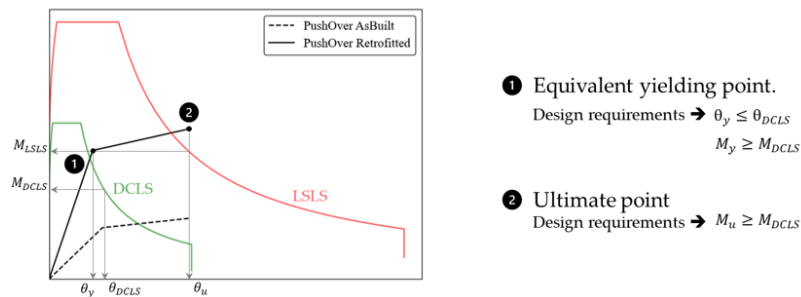


Figure 23. Design process for timber-based exoskeletons.

1. **Step 1:** Section sizes and amount of post-tension should be defined in order to ensure that the elastic deformation of the frame, θ_y , is less than the imposed limit drift for the DCLS, θ_{DCLS} . Clearly, it should also be verified that all the connections remain elastic (i.e., $M_y \geq M_{DCLS}$).
2. **Step 2:** Once Step 1 has been carried out, the procedure previously discussed can be implemented, and the detailed connection design can be carried out at the LSL (i.e., $M_u \geq M_{LSLS}$).

Finally, once the exoskeleton has been designed, another crucial point for the effectiveness of the proposed solution is the design and implementation of a reliable connection system able to transfer the shear actions from the as-built structure to the exoskeleton itself. Concerning the importance of this point, a specific chapter has been provided in this deliverable (§ 9). Here, the reader can find alternative solutions that have been developed in collaboration with Rothoblaas, industrial partner of the project, and a world-leading company in the field of connection systems for timber components.

7. NUMERICAL SIMULATIONS FOR THE RETROFITTED CONFIGURATION

7.1 Application of the DBR procedure for the design of the exoskeleton

The DBR procedure outlined in the previous section has been implemented to support the design of the low-damage exoskeleton. More specifically, non-linear static (push-over) analyses have been carried out on the retrofitted configuration, and the results have been used as input for the DBR procedure itself (i.e., for defining the design drift θ_D). Push-over analyses on the as-built configuration have been carried out both on the infilled frame as

well as on a bare frame model. The latter was used to represent the effect of the selective weakening on masonry infills described above.

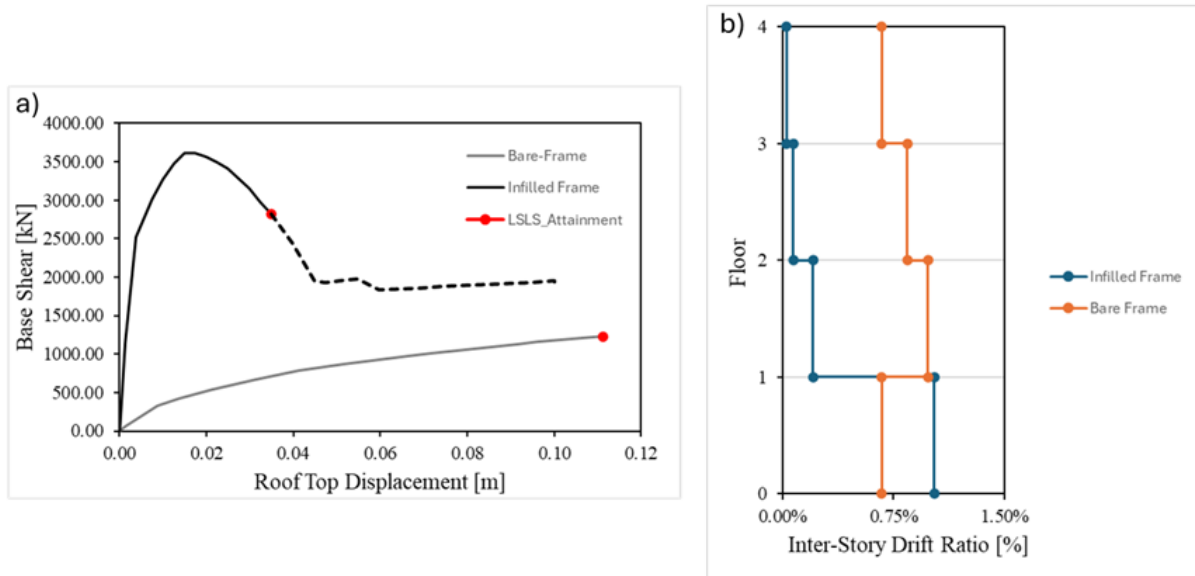


Figure 24. Results of the non-linear static analyses for the infilled and bare frame system in the as-built configuration in terms of a) push-over, and b) inter-story drift ratio at the attainment of the LSLs.

The results of these analyses are presented in Fig. 24, both in terms of a) force-displacement capacity curve (push-over) as well as in terms of b) inter-story drift at the attainment of the LSLs, and clearly show the effects of the intervention on the existing envelope. The results of the pushover analysis on the bare frame model have been used as input for the DBR procedure, and more specifically, a θ_D equal to 0.80% has been selected. Concerning the material properties of the exoskeleton, a Glulam GL30C has been considered. The mechanical characteristics of the selected material are summarized in Table 3.

| Mechanical property | Symbol | Value |
|--|--------------------------------------|-------|
| Strength in compression parallel to the grain | $f_{c,0,g,k}$ [MPa] | 24.50 |
| Modulus of elasticity parallel to the grain | $E_{0,g,Mean}$ [MPa] | 13000 |
| Modulus of elasticity perpendicular to the grain | $E_{90,g,Mean}$ [MPa] | 300 |
| Shear Modulus | $G_{g,Mean}$ [MPa] | 650 |
| Density | $\rho_{g,Mean}$ [kg/m ³] | 430 |

Table 3. Mechanical characteristics of the Glulam GL30C

Building on the results of the DBR procedure and of the detailed connection design, the considered exoskeleton is composed of structural members 68 cm in height and 32 cm in width, both for columns and beams.

After designing the exoskeleton, another numerical model of the retrofitted configuration has been implemented. More specifically, in this case, the exoskeleton has been connected in parallel to the as-built structure using rigid links representative of the connection systems between the two structures. Concerning the exoskeleton, in order to model the

non-linearities, rather than using plastic hinges, nonlinear links working in parallel at the end sections of structural members have been used, as suggested by Pampanin et al. [30]. Such links are modelled to catch the self-centring behaviour of the post-tensioning cables/bars, and the dissipation capabilities related to the Plug&Play dissipaters. More specifically, the multi-linear elastic link has been used for post-tension, while an elastic-plastic one with kinematic hysteresis rule has been adopted for modelling the Plug&Play dissipaters. Finally, an additional rotational spring has been implemented in the system of rigid links, adopted for modelling the beam-column joint, in order to capture the joint shear stiffness [31–33]. A schematic representation of the modelling approach for the retrofitted configuration is illustrated in Fig. 25.

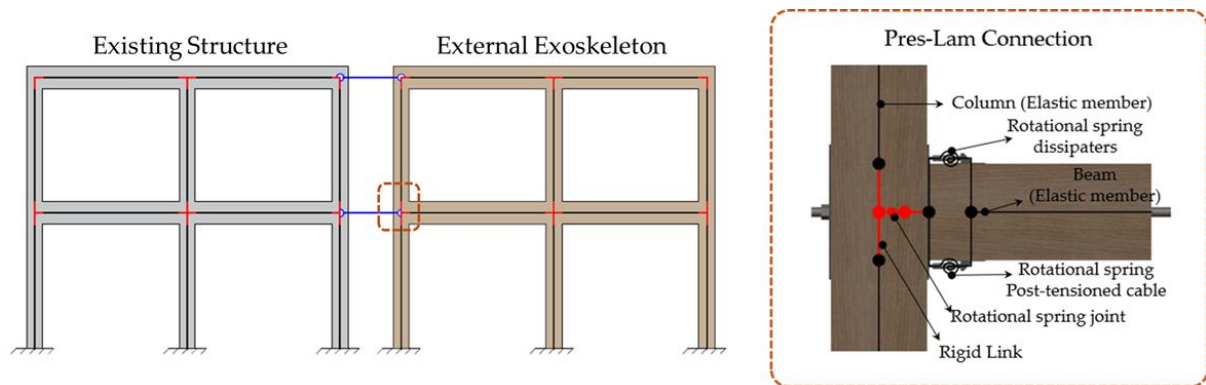


Figure 25. Modelling approach for buildings retrofitted using the low-damage exoskeleton.

Fig. 26 presents the results in terms of push-over analysis of the retrofitted structure compared with the as-built configuration (a). Moreover, an additional model of the exoskeleton has been implemented, and non-linear static cyclic analyses have been carried out in order to highlight the peculiar self-centring capabilities of the Pres-Lam exoskeleton (b).

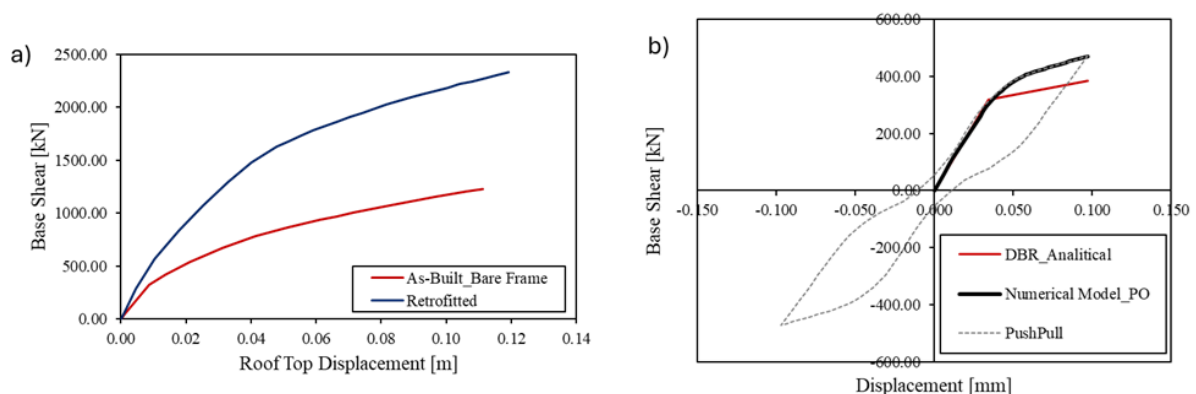


Figure 26. a) Results in terms of push-over curves for the as-built and retrofitted configuration, and b) results of cyclic non-linear static analysis (push-pull) to prove the self-centring capabilities of the external exoskeleton.

7.2 Test set-up for Pseudo-Dynamic Tests (Retrofitted Configuration)

After the tests that will be carried out on the as-built configuration, the retrofitted specimen will be realized and tested. It is worth stressing that the as-built specimen, as mentioned in §5.3, will be tested until the achievement of an acceptable level of damage, both for safety reasons in the laboratory environment, as well as to prove the effectiveness of the exoskeleton solution for the seismic retrofit of existing buildings not extensively damaged by past earthquakes (i.e. as-built structure in its undamaged configuration). More

specifically, in order to realize the retrofitted configuration, first, the selective weakening approach will be implemented on the masonry infills. After this, the timber-based low-damage exoskeleton will be attached to the RC frame. Fig. 27 presents the retrofitted specimen, together with the geometric characteristics of the exoskeleton members, while the details of the connection systems designed for the exoskeleton are presented in Fig. 28. For the PsD test to be carried out on the retrofitted configuration, the detailed description made before in § 4.1 remains valid even here.

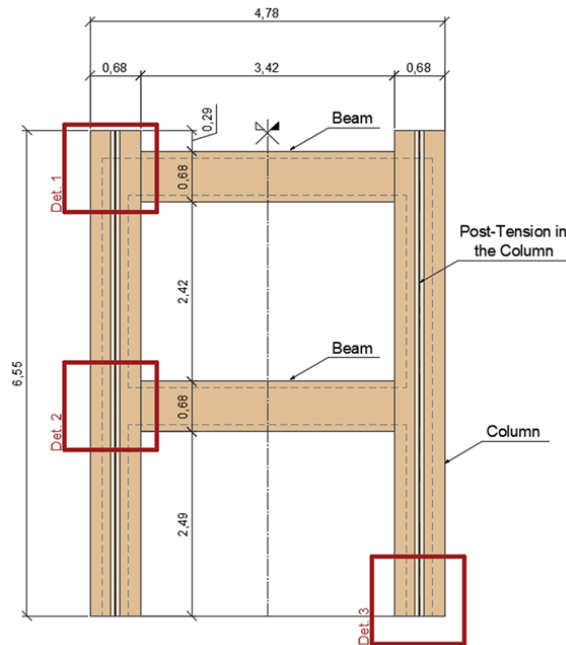


Figure 27. Geometric characteristics of the exoskeleton. Details 1 to 3 (i.e. Det. 1, Det. 2, and Det. 3) are presented in the following Fig. 28.

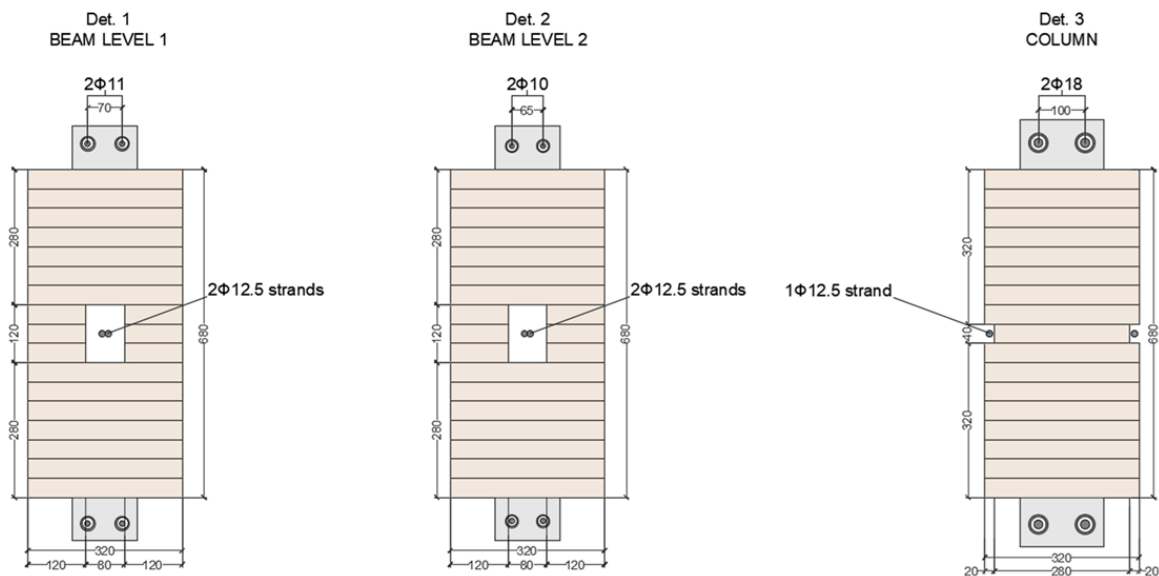


Figure 28. Details of the connection systems designed for the exoskeleton.

7.3 Substructuring approach and results from NLTHAs

As in the case of the as-built configuration, the substructuring approach has been validated following the same procedure described before (i.e., in § 5.3). NLTHAs have been conducted using several intensities, i.e., 10%, 25%, 50%, 75%, 100%, 125%, and 150% of the record selected in § 5.2. The results of the analyses show a good match between the displacement recorded at the 2nd floor, both for the whole 3D model as well as for the reinforced substructured frame, thus validating the substructuring approach even for the retrofitted configuration. The results for the intensities from 75% to 150% are shown in Fig. 29 below.

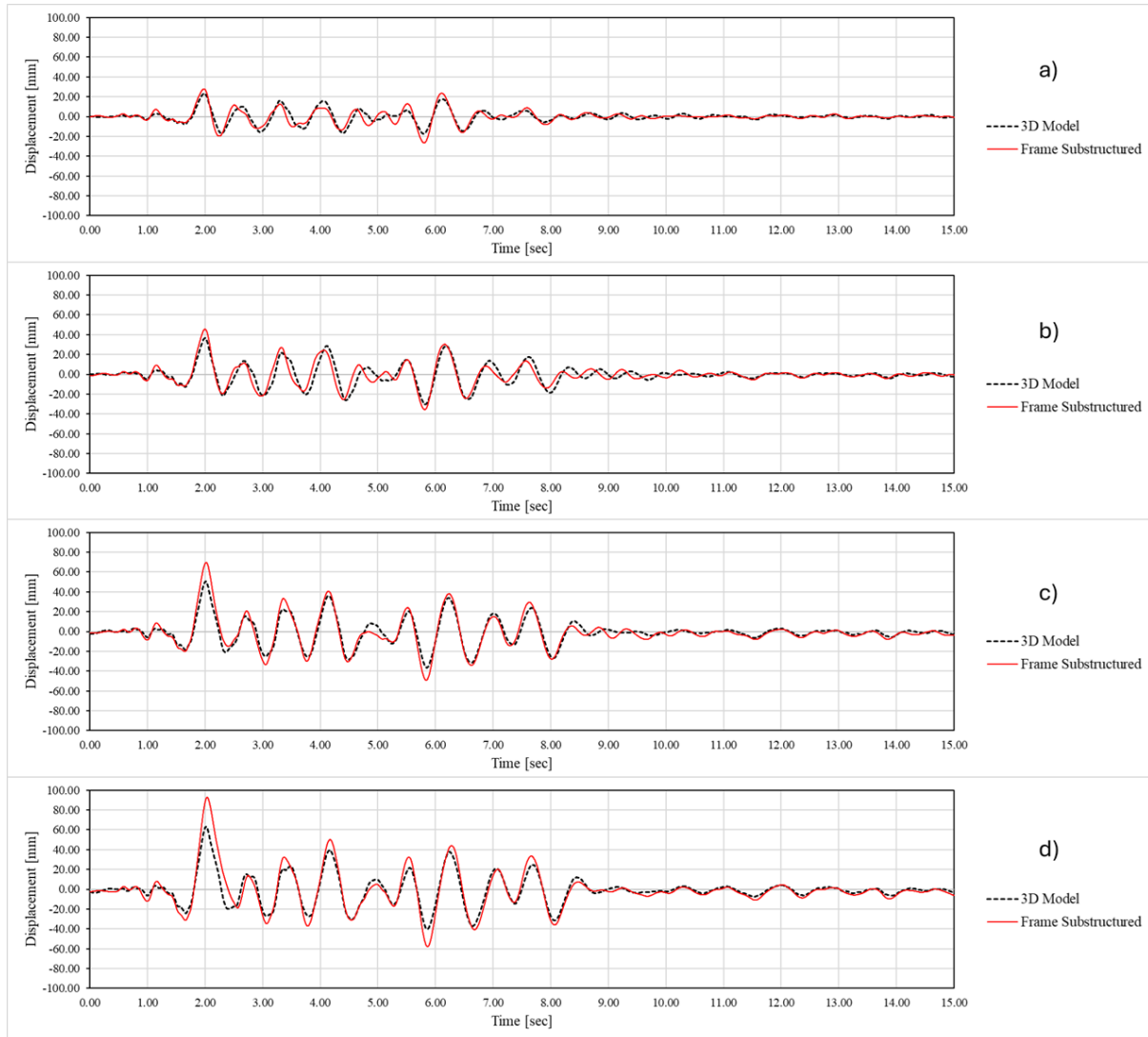


Figure 29. Comparison between the displacement recorded at the 2nd story of the whole building (3D model) and those from the substructured frame for a) 75%, b) 100%, c) 125% and d) 150% of the selected record.

8. RESILIENT CONNECTION SYSTEMS

The fastening system for the connection between the existing reinforced concrete beam and the PresLam beam must meet the following requirements:

- Maximum possible stiffness to prevent delays in the activation of the exoskeleton

- Resistance of the connection on both the concrete and timber sides to an applied force of 150 kN;
- Structural analysis based on seismic category C2 with elastic design approach;
- Positioning as far as possible from the edges to avoid interference with the dissipative beam-column joint.

Moreover, the following criteria have been considered for proposing alternative connection systems:

- **Dismantlability:** A requirement imposed by the European project to ensure a replaceable fastening system in case of damage, enhancing the life cycle of elements (LCA);
- **Product availability, cost, and additional timber processing:** These factors define the feasibility of large-scale application of the exoskeleton;
- **Exposure of screws to water:** A risk indicator for hydrogen embrittlement of metal connectors, especially relevant due to the exposure of thick plates to outdoor conditions;
- **Ease of installation:** Reduces installation times and minimizes disruption for building occupants;
- **Tolerances:** The existing beam presents significant geometric irregularities, and the fastening system should facilitate necessary geometric adjustments;
- **Architectural interferences:** The fastening geometry must avoid creating barriers for existing window and door openings.

In the following, three alternative solutions, individuated as the most suitable, are described.

8.1 Direct Anchorage (dowelled connections)

A cost-effective solution is to fasten the timber beam directly to the concrete beam using through-threaded bars and epoxy resin (Fig. 30).

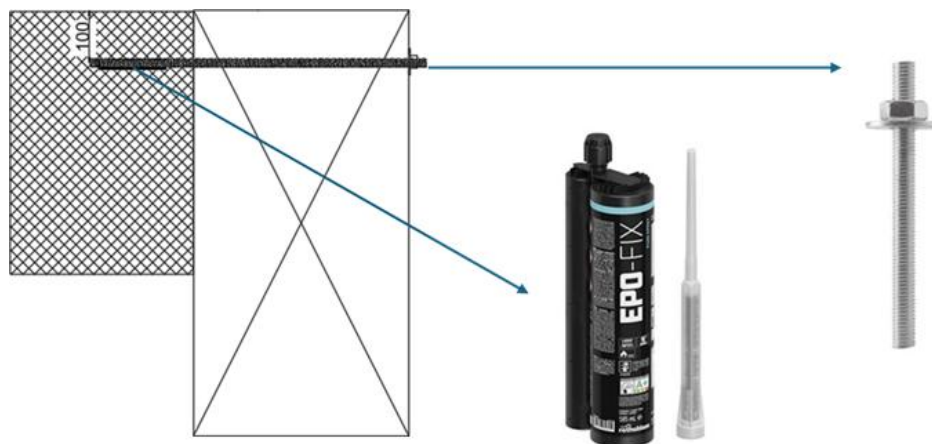


Figure 30. Dowelled Connection

The installation process involves using a template to accurately mark hole positions on the concrete, which are then transferred to the timber beam for accurate alignment. A shrinkage-free mortar is injected to fill gaps and prevent weakening of the threaded bars. Stiffness is calculated based on Eurocode 5, section 7.1, treating the bar as a bolt.

8.2 T-Profile Connection System

The connection using two T-profiles (Fig. 31) reduces potential eccentricity due to the shear transfer mechanisms between the as-built structure and the exoskeleton. Nevertheless, it should be pointed out that such a solution risks interfering with existing openings (i.e., potential architectural incompatibility). To mitigate this, at the cost of greater execution complexity, the beam can be fastened from below. If the T-profiles have sufficiently wide flanges, they allow for a certain level of construction tolerance based on the minimum edge distance of the timber beam.

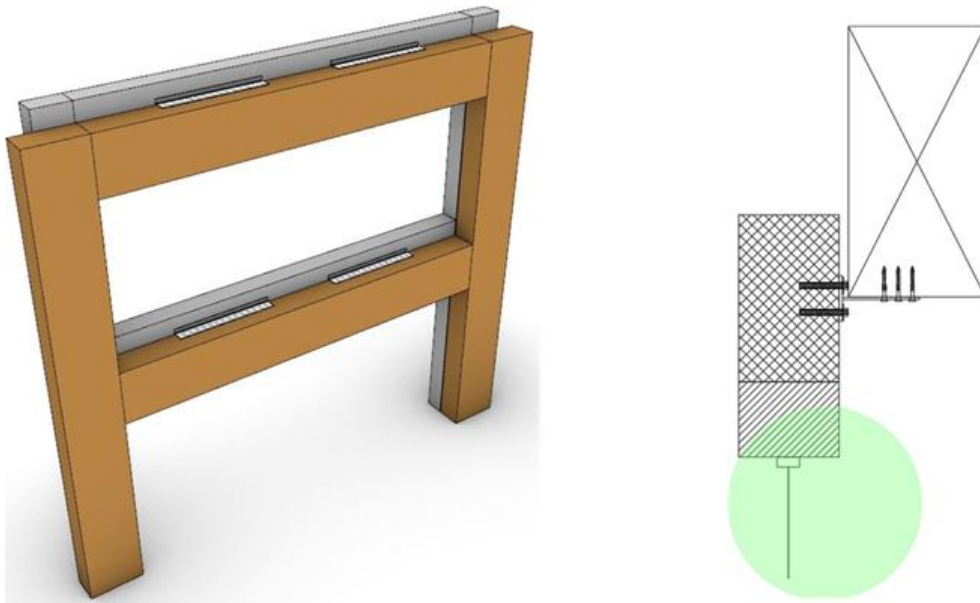


Figure 31. T-profile solution for connecting the exoskeleton to the as-built structure (left), and modification by fastening the timber beam from below, thus reducing potential architectural incompatibility (right).

8.3 Bow-Tie Connection System

This solution is an adaptation of the 'Bow Tie' connection system, already adopted in new buildings constructed by implementing the Pres-Lam technology. This connection has been adopted in such buildings for connecting seismic-resisting wall systems to floors. Like in the previous case, a metal plate is anchored with fasteners and an additional welded rectangular plate transfers forces (Fig. 32). The timber beam includes a larger through-hole to accommodate construction tolerances, through which the additional plate passes. The seismic shear force is transferred by direct contact between a steel plate and the timber beam, secured with HBSP screws. To fill any gaps and distribute forces, steel SHIM plates are introduced.

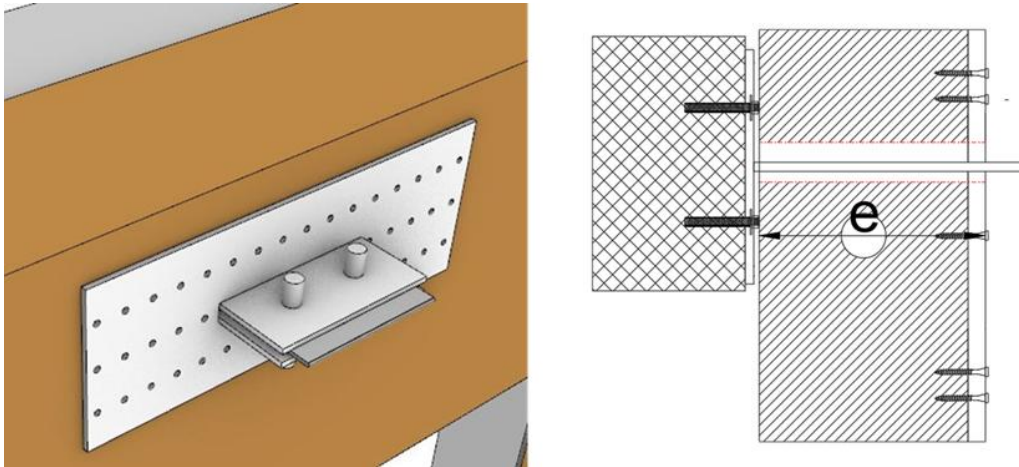


Figure 32. Schematic representation of the bow-tie connection concept. e: eccentricity.

9. REFERENCES

1. Vision S. Performance based seismic engineering of buildings. *Structural Engineers Association of California, Sacramento, Calif* 1995.
2. Pampanin S. Alternative performance-based retrofit strategies and solutions for existing RC buildings. *Seismic Risk Assessment and Retrofitting: With Special Emphasis on Existing Low Rise Structures*, Springer; 2009.
3. Palermo A, Pampanin S, Buchanan A, Newcombe M. Seismic design of multi-storey buildings using laminated veneer lumber (LVL) 2005.
4. Palermo A, Pampanin S, Buchanan AH. Experimental investigations on LVL seismic resistant wall and frame subassemblies 2006.
5. Palermo A, Pampanin S, Fragiaco M, Buchanan AH, Deam BL. Innovative seismic solutions for multi-storey LVL timber buildings 2006.
6. Priestley MJN. Overview of PRESSS research program. *PCI Journal* 1991; **36**(4): 50–57.
7. Priestley MJN, Sritharan S, Conley JR, Pampanin S. Preliminary results and conclusions from the PRESSS five-story precast concrete test building. *PCI Journal* 1999; **44**(6): 42–67.
8. Cheek GS. A hybrid reinforced precast frame for seismic regions. *PCI Journal* 1997; **42**(2): 20–32.
9. Holden T, Devereux C, Haydon S, Buchanan A, Pampanin S. NMIT Arts & Media Building—Innovative structural design of a three storey post-tensioned timber building. *Case Studies in Structural Engineering* 2016; **6**: 76–83. DOI: 10.1016/J.CSSE.2016.06.003.
10. Ramirez CM, Miranda E. Significance of residual drifts in building earthquake loss estimation 2012. DOI: 10.1002/eqe.2217.
11. Fib. *Bulletin 27: Seismic design of precast concrete building structures*. 2003.
12. Decanini LD, De Sortis A, Goretti A, Liberatore L, Mollaioli F, Bazzurro P. Performance of reinforced concrete buildings during the 2002 Molise, Italy, earthquake. *Earthquake Spectra* 2004; **20**(SPEC. 1). DOI: 10.1193/1.1765107.
13. Ministero delle infrastrutture e dei trasporti. *Aggiornamento delle Norme tecniche per le costruzioni. Gazzetta Ufficiale Serie Generale 42 (in Italian)*. Rome, Italy: 2018.
14. SAP2000 CSI. Structural analysis program. *Berkeley, California* 2005.

15. Priestley MJN, Calvi GM, Kowalsky MJ. *Direct Displacement-Based Seismic Design of Structures*. 2007.
16. New Zealand Society for Earthquake Engineering N. *Seismic Assessment of Existing Buildings Technical Guidelines for Engineering Assessments*. Wellington, New Zealand: 2017.
17. Moliterno C, Del Vecchio C, Di Ludovico M, Prota A. Pseudodynamic Tests and Numerical Modelling for Damage Analysis of Infilled RC Frames. *Journal of Earthquake Engineering* 2023; **27**(16): 4549–4574. DOI: 10.1080/13632469.2023.2183048.
18. Pampanin S, Calvi GM, Moratti M. Seismic behaviour of RC beam-column joints designed for gravity loads. *12th European Conference on Earthquake Engineering* 2002; **726**(May 2014): 1–10.
19. Panagiotakos TB, Fardis MN. Seismic Response of infilled RC Frames Structures. *11th world Conference on Earthquake Engineering*.
20. D'Amore S, Pampanin S. Displacement-based seismic retrofit of reinforced concrete buildings through low-damage exoskeletons. *Engineering Structures* 2025; **322**. DOI: 10.1016/j.engstruct.2024.119209.
21. Sgobba S, Felicetta C, Russo E, D'Amico M, Lanzano G, Pacor F, *et al.* The online graphical user interface of REXELweb for the selection of accelerograms from the Engineering Strong Motion database (ESM). *39° Convegno nazionale Gruppo Nazionale di Geofisica della Terra Solida 22–24 giugno 2021*, 2021.
22. Del Vecchio C, Di Ludovico M, Verderame GM, Prota A. Pseudo-dynamic tests on full-scale two storeys RC frames with different infill-to-structure connections. *Engineering Structures* 2022; **266**. DOI: 10.1016/j.engstruct.2022.114608.
23. Taghavi S, Miranda MM. *Response assessment of nonstructural building elements*. Pacific Earthquake Engineering Research Center; 2003.
24. O'Reilly GJ, Perrone D, Fox M, Monteiro R, Filiatrault A. Seismic assessment and loss estimation of existing school buildings in Italy. *Engineering Structures* 2018; **168**: 142–162.
25. Tasligedik AS, Pampanin S. Rocking Cantilever Clay Brick Infill Wall Panels: A Novel Low Damage Infill Wall System. *Journal of Earthquake Engineering* 2017; **21**(7): 1023–1049. DOI: 10.1080/13632469.2016.1190797.
26. Preti M, Bolis V. Masonry infill construction and retrofit technique for the infill-frame interaction mitigation: Test results. *Engineering Structures* 2017; **132**: 597–608. DOI: 10.1016/J.ENGSTRUCT.2016.11.053.
27. Priestley M. *Direct Displacement-Based Design of Precast/Prestressed Concrete Buildings*. 2002.
28. Priestley MJN, Kowalsky MJ. Direct displacement-based seismic design of concrete buildings. *Bulletin of the New Zealand Society for Earthquake Engineering* 2000; **33**(4): 421–444.
29. D'Amore S, Bianchi S, Overend M, Pampanin S. External timber-based low-damage exoskeletons for enhanced structural safety and energy efficiency. *18th World Conference on Earthquake Engineering*, 2024.
30. Pampanin S, Priestley MJN, Sritharan S. Analytical modelling of the seismic behaviour of precast concrete frames designed with ductile connections. *Journal of Earthquake Engineering* 2001; **5**(03): 329–367.
31. Smith T, Ponzo FC, Di Cesare A, Pampanin S, Carradine D, Buchanan AH, *et al.* Post-tensioned glulam beam-column joints with advanced damping systems: Testing and numerical analysis. *Journal of Earthquake Engineering* 2014; **18**(1): 147–167. DOI: 10.1080/13632469.2013.835291.

32. Di Cesare A, Ponzio FC, Nigro D, Pampanin S, Smith T. Shaking table testing of post-tensioned timber frame building with passive energy dissipation systems. *Bulletin of Earthquake Engineering* 2017; **15**(10): 4475–4498. DOI: 10.1007/s10518-017-0115-9.
33. Granello G, Leyder C, Palermo A, Frangi A, Pampanin S. Design Approach to Predict Post-Tensioning Losses in Post-Tensioned Timber Frames. *Journal of Structural Engineering* 2018; **144**(8). DOI: 10.1061/(asce)st.1943-541x.0002101.

GLOSSARY

| ACRONYM | FULL NAME |
|-----------------------|--|
| [K] | Initial Stiffness Matrix |
| [M] | Mass Matrix |
| BCJ | Beam-Column Joint |
| DBR | Displacement-Based Retrofit |
| DCLS | Damage-Control Limit-State |
| DDBD | Direct Displacement-Based Design |
| DS | Damage State |
| dt | Time step |
| FEM | Finite Element Model |
| g | Acceleration of Gravity |
| GLD | Gravity Load Design |
| HIL | Hardware In the Loop |
| IP | In-Plane |
| K_{Building} | Stiffness of the whole building |
| K_{Frame} | Stiffness of the substructured frame |
| LSLS | Life-Safety Limit-State |
| LVDT | Linear Variable Displacement Transducer |
| MRF | Moment-Resisting Frame |
| NLTHA | Non-Linear Time History Analysis |
| NZSEE | New Zealand Society for Earthquake Engineering |
| OOP | Out-of-Plane |
| PGA | Peak Ground Acceleration |
| Pres-Lam | Prestressed Laminated Timber |
| PRESSS | PREcast Seismic Structural System |
| PsD | Pseudo-Dynamic |
| RC | Reinforced Concrete |
| SEAOC | Structural Engineers Association of California |
| WS | Work-Stream |